

RIS Meets Aerodynamic HAPS: A Multi-objective Optimization Approach

Arman Azizi, *Student Member, IEEE*, Arman Farhang, *Senior Member, IEEE*

Abstract—In this paper, we propose a novel network architecture for integrating terrestrial and non-terrestrial networks (NTNs) to establish connection between terrestrial ground stations which are unconnected due to blockage. We propose a new network framework where reconfigurable intelligent surface (RIS) is mounted on an aerodynamic high altitude platform station (HAPS), referred to as aerodynamic HAPS-RIS. This can be one of the promising candidates among non-terrestrial RIS (NT-RIS) platforms. We formulate a mathematical model of the cascade channel gain and time-varying effects based on the predictable mobility of the aerodynamic HAPS-RIS. We propose a multi-objective optimization problem for designing the RIS phase shifts to maximize the cascade channel gain while forcing the Doppler spread to zero, and minimizing the delay spread upper bound. Considering an RIS reference element, we find a closed-form solution to this optimization problem based on the Pareto optimality of the aforementioned objective functions. Finally, we evaluate and show the effective performance of our proposed closed-form solution through numerical simulations.

Index Terms—RIS, NTNs, HAPS, 6G, time-varying channel.

I. INTRODUCTION

One of the most important targets in sixth generation wireless networks (6G) is the provision of ubiquitous connectivity. This aim can be attained by integration of terrestrial and non-terrestrial networks (NTNs), [1], [2]. To this end, reconfigurable intelligent surface (RIS) can be exploited to boost the channel gain by creating a multi-path environment. Non-terrestrial RIS (NT-RIS) is an intelligent intermediate reflection layer, where RIS is mounted on a non-terrestrial platform to connect the unconnected terrestrial infrastructures. Extensive research has been conducted to address the benefits of adopting NT-RIS in wireless networks, see [3]–[6] and the references therein. In practical cases, high altitude platform station (HAPS)-RIS is one of the promising candidates to be exploited for NT-RIS compared to other non-terrestrial platforms such as satellite-RIS and unmanned aerial vehicle (UAV)-RIS, [5], [6].

From the perspective of HAPS mobility, there are two types of HAPSs, aerostatic and aerodynamic, [7]. The investigation of HAPS-RIS communications is still in its infancy. The existing literature on this topic is mostly focused on aerostatic HAPS-RIS, [5], [6], [8]–[10], while the aerodynamic HAPS-RIS is left as an open research topic. The advantages of exploiting aerodynamic over aerostatic HAPS in wireless networks are well articulated in [7], e.g., low-cost and swift deployment, and high resilience to turbulence. These features make aerodynamic HAPS a promising candidate technology in

the move towards integration of terrestrial and non-terrestrial networks, [7]. However, high mobility of aerodynamic HAPS leads to time-varying channel effects. Accordingly, the main research question that arises is “*Can aerodynamic HAPS-RIS bring connectivity to the unconnected ground stations in presence of time-varying channel?*”.

There exist a number of works in the literature that consider RIS-based networks in the presence of time-varying channel, which can be classified into two groups where RIS is fixed, [11]–[13], or mobile, [14]–[16]. Our proposed network architecture in this paper falls under the area of the latter one, where the RIS is mobile. In [14] and [15], the authors present efficient Doppler shift mitigation methods, including transmission protocol and RIS phase shift control, where both of RIS and user equipment are deployed in a high-mobility terrestrial vehicle. The main difference between [14] and [15], is the design of the transmission protocol. In [16], the authors present a cooperative passive beamforming and distributed channel estimation to maximize the overall channel gain between an RIS-aided low-earth orbit satellite and a ground node. While the main focus of [14]–[16] is channel estimation, to the best of our knowledge, there is no existing work which geometrically formulates all the channel metrics and time-varying effects based on predictive mobility of RIS, which can play a vital role in reducing the computational complexity. Furthermore, the authors in [14]–[16] only consider one side of the cascade channel to be time-varying, while in this paper we investigate the case where both sides of the cascade channel are time-varying.

To summarize, this paper addresses the aforementioned gaps in the literature with the ensuing contributions: (i) We introduce a *novel network architecture* for NT-RIS assisted networks. We propose a new system model where RIS is mounted on aerodynamic HAPS to connect the unconnected terrestrial ground stations in emergency situations thanks to significant features of aerodynamic HAPS. (ii) We *mathematically model the mobility pattern of each RIS element* based on the dimensions of the RIS and the RIS elements, and the predictive trajectory of the aerodynamic HAPS-RIS. Next, we obtain a geometrical model for all the channel metrics and time-varying effects. To the best of our knowledge, there is no work which geometrically models the the mobility profile of a mobile RIS based on these parameters. (iii) We propose a multi-objective optimization problem in which the objective functions are the channel gain, the delay spread upper bound and the Doppler spread. We *obtain a closed-form solution* for the RIS phase shifts, by introducing a reference RIS element, adopting Pareto optimality. As the closed-form solution is a function of the predictive locations of RIS elements, we do not need to constantly track the channel variations and constantly update the RIS phase shifts by solving optimization problems.

The authors are with the Department of Electronic and Electrical Engineering, Trinity College Dublin, Dublin, D02 PN40 Ireland (e-mail: azizia@tcd.ie; arman.farhang@tcd.ie). This work has emanated from research supported in part by a Grant from Science Foundation Ireland under Grant number 18/CRT/6222 and Grant 13/RC/2077_P2. This work has been submitted to the IEEE for possible publication. Copyright may be transferred without notice, after which this version may no longer be accessible.

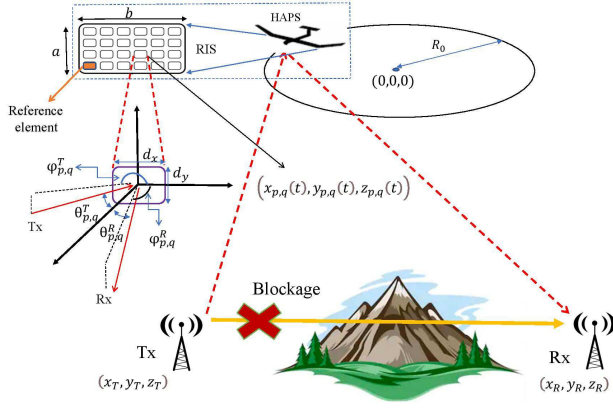


Fig. 1. Proposed network architecture based on aerodynamic HAPS-RIS.

II. SYSTEM MODEL AND PROBLEM FORMULATION

In this paper, we consider the network architecture in Fig. 1, where the link between the terrestrial transmitter (Tx) and receiver (Rx) is blocked. We consider an RIS-enabled HAPS, so-called HAPS-RIS, which is moving in a circular path with radius R_0 centered at the origin of the Cartesian coordinate system and the velocity v , see Fig. 2. We consider the RIS to be a rectangle with the length a and the width b , which is located on the bottom of the HAPS in the xy -plane. The RIS consists of $P = \lfloor \frac{a}{d_x} \rfloor$ columns and $Q = \lfloor \frac{b}{d_y} \rfloor$ rows of reflecting elements with dimensions d_x and d_y .

Definition 1. As the aerodynamic HAPS is moving in a circular path with a known speed, the geometrical mobility pattern of the RIS elements can be attained as a function of the predictive mobility of the aerodynamic HAPS, and the dimensions of the RIS and the RIS elements, as $(x_{p,q}(t), y_{p,q}(t), z_{p,q}(t)) = (R_{p,q} \cos(\frac{vt}{R_{p,q}} + \alpha_{p,q}), R_{p,q} \sin(\frac{vt}{R_{p,q}} + \alpha_{p,q}), 0)$ where

$$R_{p,q} = \sqrt{(R_0 - \frac{a}{2} + (p - \frac{1}{2})d_x)^2 + (-\frac{b}{2} + (q - \frac{1}{2})d_y)^2}, \quad (1)$$

$$\alpha_{p,q} = \arctan\left(\frac{-\frac{b}{2} + (q - \frac{1}{2})d_y}{R_0 - \frac{a}{2} + (p - \frac{1}{2})d_x}\right). \quad (2)$$

Remark 1. By observing Fig. 1 and Fig. 2, we can interpret the obtained mobility pattern of RIS elements. d_x and d_y are in the range of $[\frac{\lambda_c}{10}, \frac{\lambda_c}{5}]$ where $\lambda_c = \frac{c_0}{f_c}$ is the carrier wavelength, f_c is the carrier frequency, and c_0 is the speed of light, [17]. With these considerations, the mobility pattern in this paper is an applicable model for different carrier frequencies.

Since the line of sight (LoS) link between Tx/Rx and HAPS has the highest power, it is predominant among all the transmission paths. Therefore, we consider all the cascade paths, including ground to air (G2A) and air to ground (A2G), to be LoS, [6]. The Tx sends a passband signal $s_p(t) = \sqrt{2}\Re\{s(t) \exp(j2\pi f_c t)\} = \frac{s(t) \exp(j2\pi f_c t) + s^*(t) \exp(-j2\pi f_c t)}{\sqrt{2}}$ where $s(t)$ is the complex baseband signal with bandwidth $B/2$ which is modulated to the carrier frequency f_c satisfying $B \ll 2f_c$, [18]. Thus, the received baseband signal can be shown as $r(t) = \sum_{p=1}^P \sum_{q=1}^Q \Gamma_{p,q}(t) \exp(-j2\pi f_c \tau_{p,q}(t) - j\psi_{p,q}(t)) s(t - \tau_{p,q}(t) - \frac{\psi_{p,q}(t)}{2\pi f_c}) + n(t)$ where $\Gamma_{p,q}(t)$ is the

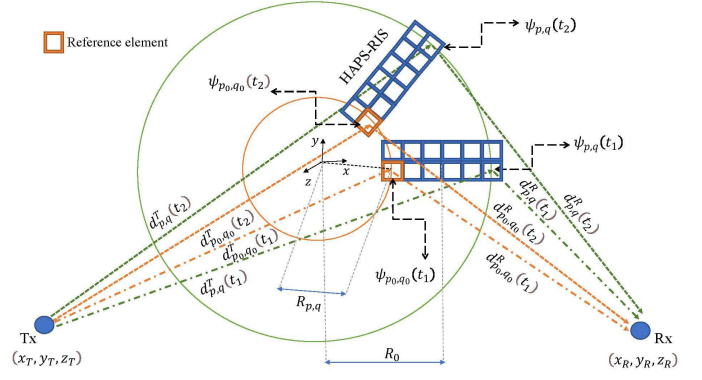


Fig. 2. Geometrical mobility pattern of RIS elements.

cascade channel gain coefficient for the RIS element (p, q) and $n(t)$ is the additive white Gaussian noise (AWGN). Additionally, $\psi_{p,q}(t)$ is the phase shift of the RIS element (p, q) . Using the Friis model, [19], $\Gamma_{p,q}(t)$ is the multiplication of the G2A and A2G amplitude gains as

$$\Gamma_{p,q}(t) = \frac{\lambda_c^2}{16\pi^2} \prod_S d_{p,q}^S(t) \sqrt{\prod_S g_S^{p,q}(t) \prod_S g_{p,q}^S(t)}, \quad (3)$$

where $S \in \{T, R\}$ represents the Tx/Rx. The distance between the RIS element (p, q) and the Tx/Rx can be calculated as $d_{p,q}^S(t) = \sqrt{(x_{p,q}(t) - x_S)^2 + (y_{p,q}(t) - y_S)^2 + (z_{p,q}(t) - z_S)^2}$. Moreover, $g_S^{p,q}(t)$ is the antenna gain of RIS element (p, q) to S , which can be a function of $\theta_{p,q}^S(t) \in [0, \pi]$ and $\varphi_{p,q}^S(t) \in [0, 2\pi]$. We consider that $g_S^{p,q}(t)$ is zero for $\theta_{p,q}^S(t) \in [\frac{\pi}{2}, \pi]$. The term $\theta_{p,q}^S(t) = \arccos(\frac{z_S - z_{p,q}(t)}{d_{p,q}^S(t)})$ is the elevation angle from the RIS element (p, q) to S . The term $\varphi_{p,q}^S(t) = \arctan(\frac{y_S - y_{p,q}(t)}{x_S - x_{p,q}(t)})$ is the azimuth angle from the RIS element (p, q) to S . Furthermore, $g_S^{p,q}(t)$ is the antenna gain of the Tx/Rx to/from the RIS element (p, q) . The terms $\theta_{p,q}^S(t)$ and $\varphi_{p,q}^S(t)$ are the angle of elevation and azimuth from S to the RIS element (p, q) , respectively. $\tau_{p,q}(t)$ is the cascade path delay for the RIS element (p, q) ,

which can be formulated as $\tau_{p,q}(t) = \frac{\sum_S d_{p,q}^S(t)}{c_0}$.

Definition 2. Considering a constant transmit signal power P_T , as in [13], the instantaneous cascade channel gain is obtained as

$$\frac{P_R(t)}{P_T} = \left| \sum_{p=1}^P \sum_{q=1}^Q \Gamma_{p,q}(t) \exp(-j2\pi f_c \tau_{p,q}(t) - j\psi_{p,q}(t)) \right|^2, \quad (4)$$

where $P_R(t)$ is the instantaneous received power.

Each cascade path through each RIS element is subject to delay and Doppler shift. When the number of RIS elements is large, the cascade channel becomes a multi-path environment, which can boost the channel gain. However, this introduces additional effects such as Doppler spread and delay spread, which need to be compensated in RIS phase shift design. Alleviating Doppler spread and delay spread at the Rx is considerably more complicated than mitigating Doppler shifts, [18]. Therefore, we alleviate the delay and Doppler spread via

appropriate RIS phase shift design and leave the Doppler shift mitigation to the Rx side.

Definition 3. The Doppler spread is obtained by finding the maximum difference in instantaneous frequency over all LoS cascade paths, as

$$B_{\text{Do}}(t) = f_c \times \max_{p,q,p',q'} \left| \frac{d}{dt} \left(\tau_{p,q}(t) + \frac{\psi_{p,q}(t)}{2\pi f_c} \right) - \frac{d}{dt} \left(\tau_{p',q'}(t) + \frac{\psi_{p',q'}(t)}{2\pi f_c} \right) \right|. \quad (5)$$

Definition 4. The delay spread is the maximum difference in propagation time over all LoS cascade paths, as follows

$$T_{\text{De}}(t) = \max_{p,q} \left\{ \tau_{p,q}(t) + \frac{\psi_{p,q}(t)}{2\pi f_c} \right\} - \min_{p,q} \left\{ \tau_{p,q}(t) + \frac{\psi_{p,q}(t)}{2\pi f_c} \right\}. \quad (6)$$

To maximize the cascade channel gain and alleviate the delay and Doppler spread resulting from RIS phase shifts, we need to maximize (4) while minimizing (5) and (6) simultaneously. On this basis, our proposed multi-objective optimization problem can be formulated as

$$\text{OP}_1 : \max_{\forall p,q: \psi_{p,q}(t)} \left[\frac{P_R(t)}{P_T} - B_{\text{Do}}(t) - T_{\text{De}}(t) \right]. \quad (7)$$

III. PROPOSED RIS PHASE SHIFT DESIGN

To find the optimal solution of OP_1 , let us consider the search space as the set Ψ . Even if we relax the continuous RIS phase shifts to discrete ones with M quantization levels, to simplify the problem, the search space has M^{PQ} states. As this is a massive number for a large number of RIS elements, finding the optimal solution is intractable in terms of computational complexity. For large values of M , to get close to the continuous case, the search space Ψ becomes prohibitively large. Thus, it is evident that if the phase shifts are continuous like our proposed scenario, solving (7) is not affordable in terms of computational complexity. To tackle this issue, we find the Pareto optimal solution of OP_1 in Proposition 1 by decomposing OP_1 into OP_2 and OP_3 . OP_2 optimizes the cascade channel gain and the Doppler spread simultaneously. Let us consider all the possible solutions of OP_2 is the solution set χ^{OP_2} . In OP_3 , we optimize the delay spread upper bound, $T_{\text{De}}^{\text{upp}}(t)$, over the feasible set $\psi \subset \chi^{\text{OP}_2}$.

Proposition 1. Let us decompose OP_1 into OP_2 and OP_3 as

$$\text{OP}_2 : \forall p, q : \psi_{p,q}(t) \in \arg \max_{\Psi} \frac{P_R(t)}{P_T} \cap \arg \min_{\Psi} B_{\text{Do}}(t), \quad (8)$$

$$\text{OP}_3 : \forall p, q : \psi_{p,q}(t) \in \arg \min_{\psi \subset \chi^{\text{OP}_2}} T_{\text{De}}^{\text{upp}}(t). \quad (9)$$

As OP_2 and OP_3 can not be optimized simultaneously, we consider that OP_2 has the higher priority order compared to OP_3 , which is elaborated later in Lemma 2. The Pareto optimal closed-form solution of (7) is

$$\psi_{p,q}(t) = 2\pi \text{mod}(f_c (\tau_{p_0,q_0}(t) - \tau_{p,q}(t)), 1), \quad (10)$$

where $\text{mod}(\mu, \eta)$ is the remainder of the division of μ by η .

Proof. The Pareto optimal solution can be attained based on lemma 1 and 2. ■

As can be seen in Fig. 2, without loss of generality, we leave aside a single reference RIS element with variable phase shift

$\psi_{p_0,q_0}(t)$, which can increase the degrees of freedom. The cascade path through the reference element is called reference path.

Lemma 1. The Doppler spread caused by the RIS elements is zero if we have

$$\frac{d}{dt} \psi_{p \neq p_0, q \neq q_0}(t) = \frac{d}{dt} \psi_{p_0,q_0}(t) + 2\pi f_c \frac{d}{dt} \varpi_{p \neq p_0, q \neq q_0}(t), \quad (11)$$

where $\varpi_{p \neq p_0, q \neq q_0}(t) = \tau_{p_0,q_0}(t) - \tau_{p \neq p_0, q \neq q_0}(t)$.

Proof. The Doppler spread can be represented as

$$B_{\text{Do}}(t) = \max\{B_{\text{Do},1}(t), B_{\text{Do},2}(t)\}, \quad (12)$$

where the Doppler spread between the reference path and other cascade paths is

$$B_{\text{Do},1}(t) = f_c \max_{p \neq p_0, q \neq q_0} \left| \frac{d}{dt} \left(\tau_{p,q}(t) + \frac{\psi_{p,q}(t)}{2\pi f_c} \right) - \frac{d}{dt} \left(\tau_{p_0,q_0}(t) + \frac{\psi_{p_0,q_0}(t)}{2\pi f_c} \right) \right|, \quad (13)$$

and the Doppler spread between the cascade paths except reference path is

$$B_{\text{Do},2}(t) = f_c \max_{p,p' \neq p_0, q,q' \neq q_0} \left| \frac{d}{dt} \left(\tau_{p,q}(t) + \frac{\psi_{p,q}(t)}{2\pi f_c} \right) - \frac{d}{dt} \left(\tau_{p',q'}(t) + \frac{\psi_{p',q'}(t)}{2\pi f_c} \right) \right|. \quad (14)$$

In order to make the Doppler spread zero, we force both $B_{\text{Do},1}$ and $B_{\text{Do},2}$ to zero, which leads to (11). ■

Lemma 2. The Pareto optimal solution, (10), optimizes (4) and (5) simultaneously, and after that minimizes $T_{\text{De}}^{\text{upp}}(t)$.

Proof. After forcing Doppler spread to zero, we have a feasible set for $\psi_{p,q}(t)$ based on (11). First, we integrate (11) with respect to t and substitute the result into (4). In the next step, in order to maximize the instantaneous cascade channel gain, all the terms of (4) should have the same phase. Therefore, $\forall p, q$ choosing

$$\psi_{p,q}(t) = \begin{cases} \psi_{p_0,q_0}(t) & p = p_0, q = q_0, \\ 2\pi f_c \varpi_{p,q}(t) + 2\pi \zeta_{p,q}(t) + \psi_{p_0,q_0}(t) & p \neq p_0, q \neq q_0, \end{cases} \quad (15)$$

and $\zeta_{p \neq p_0, q \neq q_0}(t) \in \mathbb{Z}$, maximize (4). It is clear that (4) is the most important metric among the objective functions, which leads to maximizing signal-to-noise ratio. From (11) and (15), we see that (4) and (5) can be simultaneously optimized, irrespective of the phase shift $\psi_{p_0,q_0}(t)$. Due to the causality requirement, $\psi_{p,q}(t) \geq 0$, we can attain the upper bound of delay spread based on (6) as

$$T_{\text{De}}^{\text{upp}}(t) = \max_{p,q} \left\{ \tau_{p,q}(t) + \frac{\psi_{p,q}(t)}{2\pi f_c} \right\} - \min_{p,q} \left\{ \tau_{p,q}(t) \right\}. \quad (16)$$

From (15) and (16), it is obvious that there is no single solution for optimizing OP_2 and OP_3 simultaneously. As (16) is an increasing function in $\psi_{p,q}(t)$, zero phase shift is needed $\forall p, q, t$ to minimize (16), which is impossible according to (15). Instead, there are infinite non-inferior solutions, [20]. By substituting (15) into (16), the delay spread upper bound can be obtained based on the possible solutions of OP_2 as

$$T_{\text{De}}^{\text{upp}}(t) = \max_{p \neq p_0, q \neq q_0} \left\{ \tau_{p_0,q_0}(t) + \frac{\psi_{p_0,q_0}(t)}{2\pi f_c}, \max_{p \neq p_0, q \neq q_0} \left\{ \tau_{p_0,q_0}(t) + \frac{\zeta_{p,q}(t)}{f_c} + \frac{\psi_{p_0,q_0}(t)}{2\pi f_c} \right\} \right\} - \min_{p,q} \left\{ \tau_{p,q}(t) \right\}. \quad (17)$$

In the following, we minimize the objective function in OP_3 . Based on (15) and the causality requirement, $\psi_{p,q}(t) \geq 0$, we have

$$\zeta_{p \neq p_0, q \neq q_0}(t) \geq -f_c \varpi_{p \neq p_0, q \neq q_0}(t) - \frac{\psi_{p_0, q_0}(t)}{2\pi}, \quad (18)$$

from (18) and since $\zeta_{p \neq p_0, q \neq q_0}(t) \in \mathbb{Z}$, the minimum value of $\zeta_{p \neq p_0, q \neq q_0}(t)$ can be obtained as $\zeta_{p \neq p_0, q \neq q_0}^{\min}(t) = \left\lceil -f_c \varpi_{p \neq p_0, q \neq q_0}(t) - \frac{\psi_{p_0, q_0}(t)}{2\pi} \right\rceil$ which is a decreasing function with respect to $\psi_{p_0, q_0}(t)$. Equation (17) includes additional increasing function, i.e., $\frac{\psi_{p_0, q_0}(t)}{2\pi f_c}$. By substituting $\zeta_{p \neq p_0, q \neq q_0}^{\min}(t)$ into (17), it is obvious that the variation of $\psi_{p_0, q_0}(t) \in [0, 2\pi]$ results in a small variation, less than $\frac{1}{f_c}$, in $T_{De}^{\text{upp}}(t)$. Hence, we relax $\zeta_{p \neq p_0, q \neq q_0}^{\min}(t)$ to $\zeta_{p \neq p_0, q \neq q_0}^R(t) = \left\lceil -f_c \varpi_{p \neq p_0, q \neq q_0}(t) \right\rceil$, which turns (17) into an increasing function with respect to $\psi_{p_0, q_0}(t)$. Accordingly, the closed-form solution for the RIS phase shifts are obtained as (10) by considering $\psi_{p_0, q_0}(t) = 0$ and substituting $\zeta_{p \neq p_0, q \neq q_0}^R(t)$ into (15). This closed-form solution is Pareto optimal based on Th. 4.2.1 in [21]. Accordingly, (10) jointly optimizes (4) and (5), as the first priority order, and minimizes (16) as the second priority order. Reversing the priority order between OP_2 and OP_3 , i.e., reversed priority, leads to non-efficient solution, which is presented later in Section IV. ■

Corollary 1. *With this Pareto optimal solution, the Doppler spread is zero, the maximum value for the instantaneous cascade channel gain is achieved as $\frac{P_{R}^{\max}(t)}{P_T} =$*

$$\left| \sum_{p=1}^P \sum_{q=1}^Q \Gamma_{p,q}(t) \right|^2, \text{ and the delay spread upper bound is}$$

$$T_{De}^{\text{upp}, \min}(t) = \max\{\tau_{p_0, q_0}(t), \max_{p \neq p_0, q \neq q_0} \{\tau_{p_0, q_0}(t) + \frac{\zeta_{p,q}^R(t)}{f_c}\}\} - \min_{p,q} \{\tau_{p,q}(t)\}. \quad (19)$$

IV. NUMERICAL EVALUATIONS

In this section, we evaluate the performance of our proposed RIS phase shift design in Section III. HAPS can operate in a wide range of frequency bands. We consider $f_c = 2$ GHz which is one of the dedicated International Mobile Telecommunications (IMT) bands, [7]. The aerodynamic HAPS moves in a circular trajectory, [7]. Thus, we assume a circular path with the origin $(0, 0, 0)$ and the radius $R_0 = 3$ km parallel to xy -plane. The RIS dimensions are chosen in a way such that $a = 20 \times b$, i.e., the length is much larger than the width. This is because the RIS is mounted below the HAPS wing, as in Fig. 1. Based on Remark 1, the RIS element dimensions are chosen as $d_x = d_y = \frac{\lambda_c}{5}$, and hence, the total number of RIS elements can be obtained as $P \times Q = \lceil \frac{a}{d_x} \rceil \times \lceil \frac{b}{d_y} \rceil = \lceil \frac{5a}{\lambda_c} \rceil \times \lceil \frac{a}{4\lambda_c} \rceil$. HAPS altitude and velocity of 20 km and $v = 110$ km/h are used in our simulations, respectively. These parameters are inline with the specifications of one of the well-known aerodynamic HAPS, HAWK30, [7], [22]. The terrestrial Tx and Rx coordinates in the scale of km are $(x_T, y_T, z_T) = (-5, 0, 20)$ and $(x_R, y_R, z_R) = (5, 0, 20)$, respectively. The planar antenna gain of RIS element (p, q) to S can be considered as $g_{p,q}^S(\theta_{p,q}^S(t), \varphi_{p,q}^S(t)) = \frac{4\pi}{\lambda_c^2} d_x d_y \cos \theta_{p,q}^S(t)$ for $\theta_{p,q}^S(t) \in [0, \frac{\pi}{2}]$ and zero otherwise, [13]. As the transmit and receive antennas are considered to be isotropic, $g_S^{p,q}(t) = 1$.

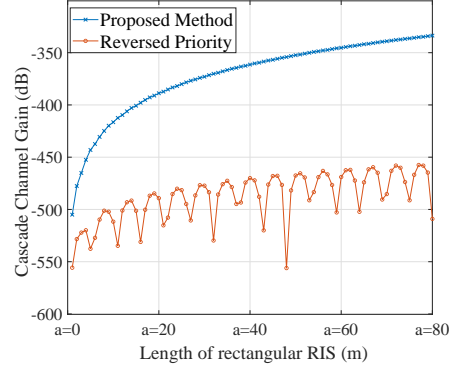


Fig. 3. Cascade channel gain versus RIS dimensions at $t = t_0$.

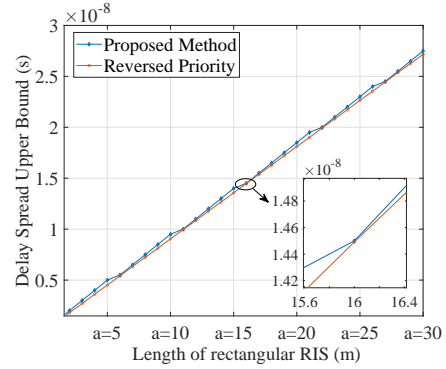


Fig. 4. Delay spread upper bound versus RIS dimensions at $t = t_0$.

As mentioned in Lemma 2, an alternative approach to our proposed method is optimization with reversed priority, i.e., reversing the order of OP_2 and OP_3 in the optimization process. Hence, in the following, we compare our proposed method with this alternative approach.

In Fig. 3 and Fig. 4, the cascade channel gain and $T_{De}^{\text{upp}}(t)$ of the proposed method and reversed approach are compared at a snapshot $t_0 = 10$ s. Using the result of Corollary 1, in Fig. 3, we plot the cascade channel gain versus RIS dimensions. As can be seen, in Fig. 3, the reversed approach leads to a poor performance compared to our proposed method. Exploiting the proposed method makes the cascade channel gain controllable and it can be constructively increased by increasing the RIS dimensions. In contrast, the cascade channel gain based on reversed approach is uncontrollable as the only controllable parameter, i.e., the RIS phase shifts are fixed. This is due to the fact, mentioning in Lemma 2, that $\psi_{p,q}(t)$ is considered zero $\forall p, q, t$ to optimize $T_{De}^{\text{upp}}(t)$ with the first priority order. By substituting $t = t_0$ s and zero phase shifts in (4), the cascade channel gain can be formulated as

$\frac{P_R(t_0)}{P_T} = \left| \sum_{p=1}^P \sum_{q=1}^Q \Gamma_{p,q}(t_0) \exp(-j2\pi f_c \tau_{p,q}(t_0)) \right|^2$. The term $\exp(-j2\pi f_c \tau_{p,q}(t_0))$ can negatively affect the cascade channel gain and makes it uncontrollable. Adopting the results of Corollary 1, in Fig. 4, we plot $T_{De}^{\text{upp}}(t_0)$ versus RIS dimensions to compare the proposed method and the reversed one. It can be seen that the delay spread gap between our proposed method and the reversed priority is negligible. Furthermore, by extrapolating Fig. 4, we can see that for $a = 80$ m, $T_{De}^{\text{upp}}(t_0)$ is around 8×10^{-8} s. This is due to the almost linear behavior

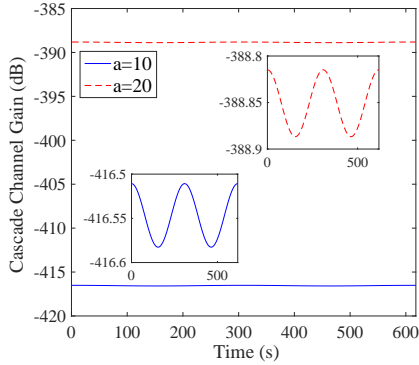


Fig. 5. Cascade channel gain versus time for different RIS dimensions.

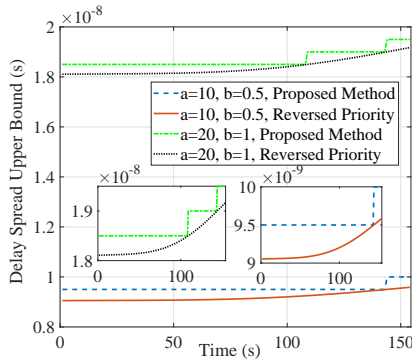


Fig. 6. Delay spread upper bound versus time for different RIS dimensions.

of $T_{De}^{upp}(t_0)$ as a function of a . Therefore, (10) can keep the delay spread upper bound controllable even for a large number of RIS elements. The claims for Fig. 3 and Fig. 4 are feasible for any $t = t_0$ based on the results presented in Figs. 5 and 6.

In Figs. 5 and 6, we analyze the cascade channel gain and $T_{De}^{upp}(t)$ versus time for different RIS dimensions, respectively. Fig. 5 shows that by increasing the value of a from 10 m to 20 m, the cascade channel gain can be increased by 27.7 dB. The small fluctuations of the cascade channel gain, due to the time-varying channel, are less than 0.1 dB, and thus, they are negligible. In Fig. 6, we plot $T_{De}^{upp}(t)$ versus time to compare our proposed method with the reversed approach. As can be seen, the gap is less than 5×10^{-10} s and it is negligible. In addition, it is clear that (10) can make $T_{De}^{upp}(t)$ controllable for different time slots.

V. CONCLUSION

In this paper, we proposed a new network architecture exploiting an aerodynamic HAPS-RIS to provide connection between the unconnected ground stations. We proposed a multi-objective optimization problem for designing the RIS phase shifts based on the predictable mobility of aerodynamic HAPS-RIS. We found a closed-form solution for the RIS phase shifts, adopting Pareto optimality, based on an RIS reference element. We maximized the channel gain, forced the Doppler spread to zero, and minimized the delay spread upper bound. By exploiting this closed-form Pareto optimal solution, we do not need to constantly track the channel variations and constantly update the RIS phase shifts by solving optimization problems. Finally, we showed the performance efficacy of our proposed closed-form solution through numerical simulation.

REFERENCES

- [1] "Study on new radio to support non-terrestrial networks," 3GPP, Sophia Antipolis, France, 3GPP Rep. TR 38.811, 2018. [Online]. Available: <https://www.3gpp.org/ftp/Specs/archive>.
- [2] M. Vaezi, A. Azari, S. Khosravirad, M. Shirvanimoghaddam, M. Azari, D. Chasaki, P. Popovski, "Cellular, wide-area, and non-terrestrial IoT: A survey on 5G advances and the road toward 6G," *IEEE Commun. Surv. Tut.*, vol. 24, no. 2, pp. 1117-1174, 2022.
- [3] J. Ye, J. Qiao, A. Kammoun, and M.S. Alouini, "Non-terrestrial communications assisted by reconfigurable intelligent surfaces," *Proc. of the IEEE*, vol. 110, no. 9, pp. 1423-1465, 2022.
- [4] P. Ramezani, B. Lyu, and A. Jamalipour, "Toward RIS-enhanced integrated terrestrial/non-terrestrial connectivity in 6G," *IEEE Network*, pp. 1-9, 2022.
- [5] S. Alfattani, W. Jaafar, Y. Hmamouche, H. Yanikomeroglu, A. Yongacoglu, N. D. Dao, and P. Zhu, "Aerial platforms with reconfigurable smart surfaces for 5G and beyond," *IEEE Commun. Mag.*, vol. 59, no. 1, pp. 96-102, 2021.
- [6] S. Alfattani, W. Jaafar, Y. Hmamouche, H. Yanikomeroglu, and A. Yongacoglu, "Link budget analysis for reconfigurable smart surfaces in aerial platforms," *IEEE Open Journal of the Commun. Soc.*, vol. 2, pp. 1980-1995, 2021.
- [7] G. Kurt, M. Khoshkholgh, S. Alfattani, A. Ibrahim, T. Darwish, M. Alam, H. Yanikomeroglu, and A. Yongacoglu, "A vision and framework for the high altitude platform station (HAPS) networks of the future," *IEEE Commun. Surv. Tut.*, vol. 23, no. 2, pp. 729-779, 2021.
- [8] S. Alfattani, A. Yadav, H. Yanikomeroglu, A. Yongacoglu, "Beyond-cell communications via HAPS-RIS," in *Proc. IEEE Globecom Workshops (GC Wkshps)*, 2022, pp. 1383-1388.
- [9] K. Tekbiyik, G. K. Kurt, C. Huang, A. R. Ekti, and H. Yanikomeroglu, "Channel estimation for full-duplex RIS-assisted HAPS backhauling with graph attention networks," in *Proc. IEEE Int. Conf. Commun. (ICC)*, Jun. 2021, pp. 1-6.
- [10] S. Alfattani, A. Yadav, H. Yanikomeroglu, A. Yongacoglu, "Resource-efficient HAPS-RIS enabled beyond-cell communications," *IEEE Wireless Commun. Lett.*, 2023.
- [11] S. Sun and H. Yan, "Channel estimation for reconfigurable intelligent surface-assisted wireless communications considering Doppler effect," *IEEE Wireless Commun. Lett.*, vol. 10, no. 4, pp. 790-794, Apr. 2021.
- [12] Z. Huang, B. Zheng, and R. Zhang, "Roadside IRS-aided vehicular communication: efficient channel estimation and low-complexity beamforming design," *arXiv preprint arXiv:2207.03157*, Jul. 2022.
- [13] B. Matthiesen, E. Björnson, E. De Carvalho, and P. Popovski, "Intelligent reflecting surface operation under predictable receiver mobility: A continuous time propagation model," *IEEE Wireless Commun. Lett.*, vol. 10, no. 2, pp. 216-220, 2020.
- [14] W. Wu, H. Wang, W. Wang, and R. Song, "Doppler mitigation method aided by reconfigurable intelligent surfaces for high-speed channels," *IEEE Wireless Commun. Lett.*, vol. 11, no. 3, pp. 627-631, 2022.
- [15] Z. Huang, B. Zheng, and R. Zhang, "Transforming fading channel from fast to slow: Intelligent refracting surface aided high-mobility communication," *IEEE Trans. Wireless Commun.*, vol. 21, no. 7, pp. 4989-5003, Jul. 2022.
- [16] B. Zheng, S. Lin, and R. Zhang, "Intelligent reflecting surface-aided LEO satellite communication: Cooperative passive beamforming and distributed channel estimation," *IEEE JSAC*, vol. 40, no. 10, pp. 3057-3070, Oct. 2022.
- [17] Ö. Özdogan, E. Björnson, and E. G. Larsson, "Intelligent reflecting surfaces: Physics, propagation, and pathloss modeling," *IEEE Wireless Commun. Lett.*, vol. 9, no. 2, pp. 581-585, May 2020.
- [18] E. Björnson, H. Wymeersch, B. Matthiesen, P. Popovski, L. Sanguinetti, and E. Carvalho "Reconfigurable intelligent surfaces: A signal processing perspective with wireless applications," *IEEE Signal Process. Mag.*, vol. 39, no. 2, pp. 135-158, 2022.
- [19] H. T. Friis, "A note on a simple transmission formula," *Proc. of the IRE*, vol. 34, no. 5, pp. 254-256, 1946.
- [20] E. Björnson, E. A. Jorswieck, M. Debbah, and B. Ottersten, "Multi-objective signal processing optimization: The way to balance conflicting metrics in 5G systems," *IEEE Signal Process. Mag.*, vol. 31, no. 6, pp. 14-23, 2014.
- [21] K. Miettinen, *Nonlinear Multiobjective Optimization*. Boston, MA, USA: Springer, 1999.
- [22] HAPSMobile. Accessed: Nov. 24, 2022. [Online]. Available: <https://www.hapsmobile.com/>